

CrystEngComm

Accepted Manuscript



This is an *Accepted Manuscript*, which has been through the Royal Society of Chemistry peer review process and has been accepted for publication.

Accepted Manuscripts are published online shortly after acceptance, before technical editing, formatting and proof reading. Using this free service, authors can make their results available to the community, in citable form, before we publish the edited article. We will replace this *Accepted Manuscript* with the edited and formatted *Advance Article* as soon as it is available.

You can find more information about *Accepted Manuscripts* in the [Information for Authors](#).

Please note that technical editing may introduce minor changes to the text and/or graphics, which may alter content. The journal's standard [Terms & Conditions](#) and the [Ethical guidelines](#) still apply. In no event shall the Royal Society of Chemistry be held responsible for any errors or omissions in this *Accepted Manuscript* or any consequences arising from the use of any information it contains.

Cite this: DOI: 10.1039/c0xx00000x

www.rsc.org/xxxxxx

ARTICLE TYPE

Functionalities and Architectures of Coordination Polymers with Multi-Dimensionalities via Transition Metals–Dicarboxylate Ligands

Xinyu Cao, Ling Li, Changxia Li, Lei Lv, Rudan Huang*

Five coordination polymers, namely, $\text{Zn}(\text{dpd})(\text{bpy})_{0.5}$ (**1**), $\text{Zn}(\text{Hdpd})_2(\text{bpy})_2 \cdot \text{H}_2\text{O}$ (**2**), $\text{Co}_3(\text{Hdpd})_2(\text{dpd})_2(\text{bpy})_3(\text{H}_2\text{O})_2 \cdot 2\text{H}_2\text{O}$ (**3**), $\text{Co}(\text{Hdpd})_2(\text{bpy})(\text{H}_2\text{O})_2 \cdot 2\text{H}_2\text{O}$ (**4**), $\text{Ni}(\text{Hdpd})_2(\text{bpy})(\text{H}_2\text{O})_2 \cdot 2\text{H}_2\text{O}$ (**5**) (H_2dpd = 2,4–diphenyl ether dicarboxylic acid, bpy = 4,4'–bipyridine) with zero– (0D), one– (1D), two– (2D) and three–dimensional (3D) structures have been synthesized under similar hydrothermal conditions by H_2dpd , bpy and different transition metal salts. Compound **1** displays a 3D framework with $\{4 \cdot 8^2\} \{4 \cdot 8^2 \cdot 10^3\}$ topology. Compound **2** is a mononuclear structure which is further self–assembled through both hydrogen bonding and $\pi \cdots \pi$ stacking interactions to generate a 3D supramolecular structure. Compound **3** shows a 2D ladder network with $\{4 \cdot 6^2\}_2 \{4^2 \cdot 6^2 \cdot 8^2\}$ topology, which consists of 1D ladder–like chains. Compounds **4** and **5** are isostructural and feature 1D chains which are further connected by hydrogen bonding interactions to form 2D supramolecular structures. These compounds have been characterized by elemental analysis, infrared (IR), thermal gravimetric analysis (TGA), and single crystal X–ray diffraction. Furthermore, fluorescence properties of **1–5** have been investigated. The water vapor sorption studies reveal compounds **3**, **4** and **5** exhibit very good water vapor uptakes (100.71 ml/g for **3**, 109.94 ml/g for **4** and 108.96 ml/g for **5**). Magnetic susceptibility measurements indicate that compounds **3** and **4** show antiferromagnetic interactions, while compound **5** shows ferromagnetic behavior.

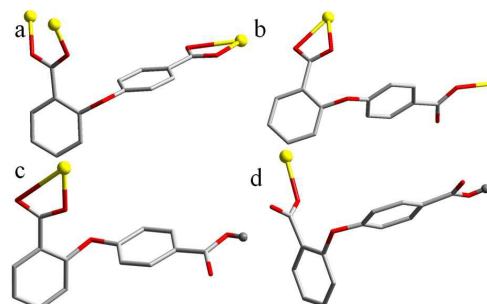
Introduction

In recent years, the design and synthesis of metal–organic coordination polymers have attracted intense interest in the world owing to their diverse structures and excellent functional applications such as sorption,¹ separation,² luminescence³ and magnetism⁴. Until now, a large number of metal–organic coordination polymers with various structures have been synthesized.⁵ Since many factors such as coordination modes of different metal atoms, the configuration, rigidity, substituent and coordination modes of the organic ligands may influence the final structures of coordination polymers except for external factors, it is still a major challenge to find regular rules for tuning the structural dimensions.^{6–10}

Among the present contributions, carboxylate–based ligands have played very important roles in the synthesis of coordination polymers. They can form diverse structures such as 0D cages, 1D chains, 2D grids and 3D porous frameworks with different metal ions.¹¹ Our group tried to tune the structural dimensions of coordination polymers by a flexible 2,4–diphenyl ether dicarboxylic acid (H_2dpd) and rigid 4,4'–bipyridine ligands (bpy). H_2dpd has two carboxyl groups which can be completely or partially deprotonated, adopting versatile coordination modes and resulting in many interesting structures with different dimensions (Scheme 1). In addition, H_2dpd and bpy ligands are also excellent hydrogen bond donors and acceptors to construct novel structures, which can interact with small molecules especially water molecules via strong hydrogen bonds.¹² We tried to explore the water vapor sorption applications of the coordination polymers based on carboxylate ligands after the

solvent removal, which turned out to be perfect candidates for water vapor sorption since water molecules are easily to be encapsulated in the structures through hydrogen bonds.¹³

In this paper, five novel structures were obtained, namely, $\text{Zn}(\text{dpd})(\text{bpy})_{0.5}$ (**1**), $\text{Zn}(\text{Hdpd})_2(\text{bpy})_2 \cdot \text{H}_2\text{O}$ (**2**), $\text{Co}_3(\text{Hdpd})_2(\text{dpd})_2(\text{bpy})_3(\text{H}_2\text{O})_2 \cdot 2\text{H}_2\text{O}$ (**3**), $\text{Co}(\text{Hdpd})_2(\text{bpy})(\text{H}_2\text{O})_2 \cdot 2\text{H}_2\text{O}$ (**4**), $\text{Ni}(\text{Hdpd})_2(\text{bpy})(\text{H}_2\text{O})_2 \cdot 2\text{H}_2\text{O}$ (**5**) based on the flexible 2,4–diphenyl ether dicarboxylic acid and rigid 4,4'–bipyridine ligand. These compounds are characterized by elemental analysis, IR, TGA, and single crystal X–ray diffraction. Fluorescence properties, water vapor sorption measurements, AC Impedance and magnetic properties of these materials are also discussed.



Scheme 1 Coordination modes of H_2dpd ligand in compounds **1–5**

Experimental section

Materials and methods

All reagents and solvents were purchased commercially and used as–purchased without further purification. Elemental analysis for

C, H and N were carried out with a Perkin–Elmer 2400 CHN elemental analyzer. The IR spectra were recorded (as KBr pressed pellets) in the range of 400–4000 cm^{-1} on a Nicolet 170SXFT–IR spectrometer. Thermal gravimetric analysis data were collected on a Perkin–Elmer TGA 7 instrument in nitrogen at a heating rate of 10 $^{\circ}\text{C}/\text{min}$. The PXRD diagrams were collected by a Shimadzu XRD–6000 diffractometer. Fluorescence spectra were measured by a Hitachi Model RF–5301 PC fluorescence spectrophotometer with a Xenon lamp light source. Water vapor sorption studies were determined by an IGA-100 gravimetric analyzer (Hidden Isochema Ltd.) AC impedance measurements were carried out with Agilent 4294A Precision Impedance Analyzer. The magnetic measurements were performed on the Quantum Design SQUID MPMSXL–7 instruments in a magnetic field of 1000 Oe in the temperature range of 2–300 K.

Synthesis of $\text{Zn}(\text{dpd})(\text{bpy})_{0.5}$ (**1**)

A mixture of $\text{Zn}(\text{OAc})_2 \cdot 4\text{H}_2\text{O}$ (0.2 mmol, 0.0590 g), H_2dpd (0.2 mmol, 0.0512 g), bpy (0.2 mmol, 0.0312 g), 25% $(\text{C}_2\text{H}_5)_4\text{NOH}$ (mass fraction) aqueous solution (0.1 ml) and H_2O (5 mL) was sealed in a 23 mL Teflon–lined autoclave and heated to 160 $^{\circ}\text{C}$ for 3 days. After cooling to room temperature at a speed of 10 $^{\circ}\text{C}/\text{h}$, colorless block crystals of compound **1** were obtained, washed with H_2O and dried in air (Yield: 45% based on Zn). Anal. Calc. for $\text{C}_{19}\text{H}_{12}\text{ZnNO}_5$: C, 57.09; H, 3.03; N, 3.50. Found: C, 57.06; H, 3.19; N, 3.45. IR (KBr, cm^{-1}): $\nu = 3460$ (w), 2932 (w), 1631 (s), 1597 (s), 1398 (m), 1240 (s), 1097 (w), 1012 (w), 879 (m), 598 (m), 504 (w).

Synthesis of $\text{Zn}(\text{Hdpd})_2(\text{bpy})_2 \cdot \text{H}_2\text{O}$ (**2**)

The synthetic procedure was similar to that of **1**, except the temperature was adjusted to 110 $^{\circ}\text{C}$. The pale yellow block crystals were obtained, washed with H_2O and dried in air (Yield: 7% based on Zn). Anal. Calc. for $\text{C}_{48}\text{H}_{36}\text{ZnN}_4\text{O}_{11}$: C, 63.34; H, 3.98; N, 6.16. Found: C, 63.26; H, 3.89; N, 6.05. IR (KBr, cm^{-1}): $\nu = 3470$ (w), 2935 (w), 1626 (s), 1595 (s), 1392 (s), 1246 (s), 1118 (w), 1007 (w), 879 (w), 581 (m), 513 (w).

Synthesis of $\text{Co}_3(\text{Hdpd})_2(\text{dpd})_2(\text{bpy})_3(\text{H}_2\text{O})_2 \cdot 2\text{H}_2\text{O}$ (**3**)

The synthetic procedure was similar to that of **1**, except

Table 1. Crystal and X-ray experimental data for **1–5**.

	1	2	3	4	5
Empirical formula	$\text{C}_{19}\text{H}_{12}\text{ZnNO}_5$	$\text{C}_{48}\text{H}_{36}\text{ZnN}_4\text{O}_{11}$	$\text{C}_{86}\text{H}_{66}\text{Co}_3\text{N}_6\text{O}_{24}$	$\text{C}_{38}\text{H}_{34}\text{CoN}_2\text{O}_{14}$	$\text{C}_{38}\text{H}_{34}\text{NiN}_2\text{O}_{14}$
M	399.69	910.18	1744.24	801.60	801.38
crystal system	monoclinic	triclinic	monoclinic	monoclinic	monoclinic
space group	P2(1)/n	P–1	P2(1)/n	P2/n	P2/n
<i>a</i> (Å)	8.3355(7)	10.1894(13)	9.9601(5)	12.3741(6)	12.4477(10)
<i>b</i> (Å)	10.7168(9)	10.3988(13)	32.5682(13)	11.3562(5)	11.2748(7)
<i>c</i> (Å)	19.0538(18)	21.838(2)	12.2300(5)	13.6838(8)	13.6629(16)
α ($^{\circ}$)	90	92.912(9)	90	90	90
β ($^{\circ}$)	95.0940(10)	103.316(10)	107.435(2)	107.309(2)	107.632(2)
γ ($^{\circ}$)	90	111.412(12)	90	90	90
<i>Z</i>	2	2	2	2	2
<i>D</i> (Mg/m^3)	1.566	1.458	1.530	1.450	1.456
μ (mm^{-1})	1.479	0.663	0.738	0.541	0.604
<i>F</i> (000)	812	940	1794	830	832
<i>R</i> ₁ (<i>I</i> > 2 σ (<i>I</i>))	0.0430	0.0647	0.0414	0.0437	0.0535
<i>R</i> ₁ (all data)	0.0879	0.1470	0.0633	0.0639	0.1014
w <i>R</i> ₂ (<i>I</i> > 2 σ (<i>I</i>))	0.0593	0.0746	0.0831	0.0951	0.0940
w <i>R</i> ₂ (all data)	0.0673	0.1058	0.0933	0.1084	0.1207
GOF on <i>F</i> ²	0.957	0.932	1.048	1.029	1.042

$\text{Co}(\text{OAc})_2 \cdot 4\text{H}_2\text{O}$ (0.2 mmol, 0.0498 g) replaced $\text{Zn}(\text{OAc})_2 \cdot 4\text{H}_2\text{O}$. The purple crystals were obtained, washed with H_2O and dried in air (Yield: 63% based on Co). Anal. Calc. for $\text{C}_{86}\text{H}_{66}\text{Co}_3\text{N}_6\text{O}_{24}$: C, 59.22; H, 3.81; N, 4.82. Found: C, 59.26; H, 3.79; N, 4.85. IR (KBr, cm^{-1}): $\nu = 3458$ (w), 2954 (m), 1686 (w), 1537 (s), 1364 (m), 1212 (s), 1098 (w), 987 (m), 883 (s), 592 (m), 516 (w).

Synthesis of $\text{Co}(\text{Hdpd})_2(\text{bpy})(\text{H}_2\text{O})_2 \cdot 2\text{H}_2\text{O}$ (**4**)

The synthetic procedure was similar to that of **3**, except the temperature was adjusted to 110 $^{\circ}\text{C}$. The orange block crystals were obtained, washed with H_2O and dried in air (Yield: 68% based on Co). Anal. Calc. for $\text{C}_{38}\text{H}_{34}\text{CoN}_2\text{O}_{14}$: C, 56.94; H, 4.28; N, 3.49. Found: C, 56.86; H, 4.29; N, 3.45. IR (KBr, cm^{-1}): $\nu = 3463$ (w), 2922 (w), 1675 (s), 1507 (w), 1390 (w), 1063 (w), 776 (m), 606 (m), 434 (w).

Synthesis of $\text{Ni}(\text{Hdpd})_2(\text{bpy})(\text{H}_2\text{O})_2 \cdot 2\text{H}_2\text{O}$ (**5**)

The synthetic procedure was similar to that of **4** except $\text{Ni}(\text{OAc})_2 \cdot 6\text{H}_2\text{O}$ (0.2 mmol, 0.0590g) replaced $\text{Co}(\text{OAc})_2 \cdot 4\text{H}_2\text{O}$. The pale green crystals were obtained, washed with H_2O and dried in air (Yield: 43% based on Ni). Anal. Calc. for $\text{C}_{38}\text{H}_{34}\text{NiN}_2\text{O}_{14}$: C, 56.95; H, 4.27; N, 3.50. Found: C, 57.06; H, 4.29; N, 3.55. IR (KBr, cm^{-1}): $\nu = 3460$ (w), 2927 (w), 1676 (s), 1506 (s), 1394 (s), 1089 (w), 769 (m), 603 (m), 455 (w).

Single-crystal X-ray crystallography

Diffraction data for **1–5** were collected on a Bruker Smart Apex CCD diffractometer by graphite–monochromated Mo–*K* α radiation ($\lambda = 0.71073$ Å). Empirical absorption corrections were taken from SADABS.¹⁴ Space group was determined by using XPREP.¹⁵ Structures were solved by direct methods and refined on *F*² with full–matrix least–squares method using the SHELXS–97 and SHELXL–97.¹⁶ Crystallographic data for compounds **1–5** were summarized in Table 1. Selected bond lengths and angles are given in Table S1, ESI. Hydrogen bonding interactions of **1–5** are given in Table S2, ESI. These data can be obtained free of charge from the Cambridge Crystallographic Data Centre via www.ccdc.cam.ac.uk/data_request/cif.

Cite this: DOI: 10.1039/c0xx00000x

www.rsc.org/xxxxxx

ARTICLE TYPE

Results and Discussion

Synthesis

Compounds **1–5** reported here were obtained by the combination of H₂dpd, bpy and three different transition metal salts under similar hydrothermal conditions. Compounds **1** and **3** were synthesized with the reactants mole ratio of 1:1:1 at 160 °C, while adjusting the reaction temperature to 110 °C, compounds **2**, **4** and **5** were obtained. Obviously, compounds **1** and **3** have higher structural dimensionalities than **2**, **4** and **5**, indicating that reaction temperature may have an important influence on the final structures. In addition, different coordination modes of H₂dpd ligand also play important roles in **1–5**, which can be a feasible method to adopt proper ligands to construct coordination polymers with target structures.

Crystal structure of compound **1**

Single crystal X-ray diffraction analysis reveals that compound **1** crystallizes in the monoclinic crystal system $P2(1)/n$. The asymmetric unit contains one Zn(II) atom, one dpd²⁻ ligand and half a bpy ligand. As shown in Fig. 1a, the Zn(II) atom is five-coordinated by four oxygen atoms from three dpd²⁻ ligands and one nitrogen atom from one bpy ligand in a distorted pyramidal coordination geometry. The Zn–O bond lengths are in the range of 1.930 to 2.559 Å, and the Zn–N bond length is 2.003 Å. The dpd²⁻ ligand in compound **1** presents a dihedral angle of 76.99° between the two benzene rings, which is nearly vertical. Adjacent Zn(II) atoms are connected by two carboxyl groups of two different dpd²⁻ ligands into a dinuclear [Zn₂(CO₂)₂] ring with a Zn···Zn distance of 3.614 Å, which are further linked dpd²⁻ ligands into a 2D layer (Fig. 1b). The adjacent layers are connected by bpy ligands into a 3D structure. The completely deprotonated bpd²⁻ ligand adopts both bridging and chelating coordination modes in compound **1** (Scheme 1a). The Zn(II) atom connects three dpd²⁻ ligands and one bpy ligand, which can be simplified as a 4-connected node. Then, each dpd²⁻ ligand connects three Zn(II) atoms as a 3-connected node. Thus, the whole framework of compound **1** can be considered as a (3,4)-connected net with the point symbol of {4·8²}{4·8²·10³} (Fig. 1c).

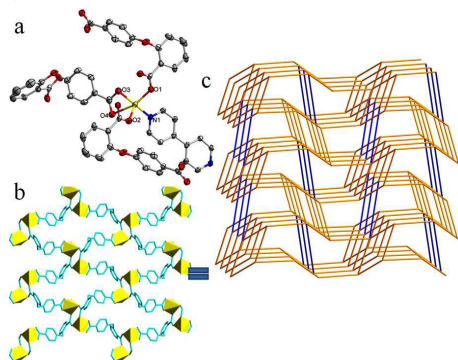


Fig. 1 (a) The coordination environment of Zn(II) in **1** with the ellipsoids drawn at the 30% probability level. (b) 2D layer of **1**, viewed along the *a* axis. (c) 3D structure of **1**.

Crystal structure of compound **2**

Compound **2** shows a mononuclear structure, and crystallizes in the triclinic space group of $P\bar{1}$. The asymmetric unit contains one Zn(II) atom, two Hdpd⁻ ligands and two bpy ligands. Unlike the compounds above, the Hdpd⁻ ligand in compound **2** is partially deprotonated, so only one carboxyl group can chelate to the Zn(II) atom (Scheme 1c). The Zn(II) atom is six-coordinated by four oxygen atoms from two Hdpd⁻ ligands and two nitrogen atoms from two bpy ligands in a distorted octahedral coordination geometry (Fig. 2a). The bond lengths of Zn–O and Zn–N are 1.956 to 2.167 Å and 2.095 to 2.096 Å, respectively. The monomers of compound **2** are connected together by the intermolecular hydrogen bonding interactions between the uncoordinated oxygen atoms of the carboxyl groups and the oxygen atoms of the lattice water molecules to form a 1D supramolecular chain (Fig. 2b). The O···O distances are 2.560 to 2.766 Å. These chains are further connected by the hydrogen bonding interactions between the nitrogen atoms and the uncoordinated oxygen atoms from the carboxyl groups into a 2D supramolecular layer (Fig. 2c). The N···O distances are 2.691 and 2.819 Å. Finally, these 2D layers are linked by the $\pi\cdots\pi$ stacking interactions between the nearby benzene rings with the distances between 3.797 to 3.900 Å to form a 3D supramolecular structure along *b* axis (Fig. 2d).

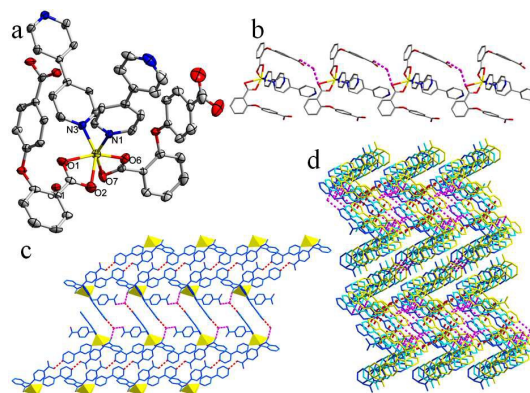


Fig. 2 (a) The coordination environment of Zn(II) in **2** with the ellipsoids drawn at the 30% probability level. (b) 1D supramolecular chain of **2**. (c) 2D supramolecular layer of **2**. (d) 3D supramolecular structure of **2** constructed by hydrogen bonding and $\pi\cdots\pi$ stacking interactions.

Crystal structure of compound **3**

Compound **3** crystallizes in the monoclinic space group $P2(1)/n$ revealing a 2D ladder structure. There are three Co(II) atoms, two Hdpd⁻ ligands, two dpd²⁻ ligands, three bpy ligands, two coordinated water molecules and two lattice water molecules in the asymmetric unit. There exist two types of crystallographically independent Co(II) atoms in compound **3** (Fig. 3a). Co1 atom is six-coordinated in a distorted octahedral coordination geometry completed by two oxygen atoms from one dpd²⁻ ligands, two oxygen atoms from Hdpd⁻ ligands and two nitrogen atoms from two bpy ligands. Co2 atom is six-coordinated in a distorted octahedral coordination geometry, with the equatorial sites occupied by two oxygen atoms from two dpd²⁻ ligands and two nitrogen atoms from two bpy ligands. The two axial sites are taken up by two oxygen atoms from two coordinated water molecules. The bond lengths of Co–O and Co–N are 2.042 to 2.092 Å and 2.100 to 2.191 Å, respectively. Unlike the compounds above, one type of dpd²⁻ ligands is completely deprotonated, exhibiting both chelating and monodentate bridging coordination modes (Scheme 1b). The other type of Hdpd⁻ ligand is partially deprotonated, exhibiting a chelating coordination mode (Scheme 1c). The Co(II) atoms are connected by the bpy ligands into a 1D ladder-like chain (Fig. 3b). These chains are further linked together by the dpd²⁻ ligands into a 2D ladder structure. From a topological perspective, the Co1 atom can be regarded as a 3-connected node and the Co2 atom can be simplified as a 4-connected node. Thus, the whole structure can be topologically represented as a (3, 4)-connected net with the vertex symbol of $\{4\cdot 6^2\}_2\{4^2\cdot 6^2\cdot 8^2\}$ (Fig. 3c).

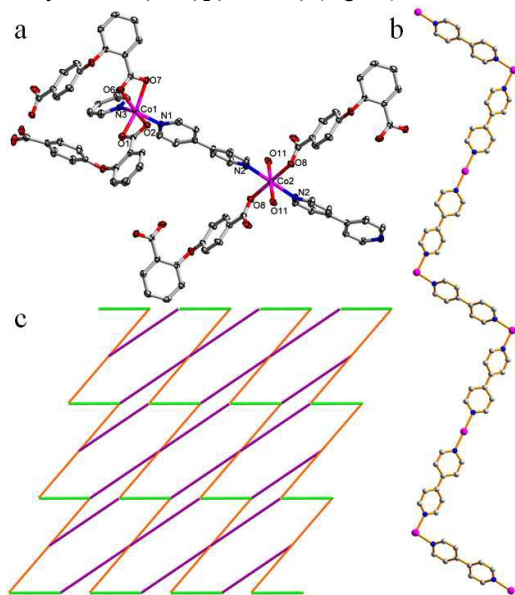


Fig. 3 (a) The coordination environment of Co(II) in **3** with the ellipsoids drawn at the 30% probability level. (b) 1D ladder chain of **3**, viewed along the *c* axis. (c) topology of **3**.

Crystal structure of compound **4**

Single crystal structure analysis reveals that compounds **4** and **5** are isostructural and crystallize in the monoclinic crystal system with $P2/n$ space group. Hence, only the structure of **4** will be described as a representative example here and the structural figure of crystal **5** can be found in the Supporting Information (Figure S1). There are one Co(II) atom, two Hdpd⁻ ligands, one

bpy ligand, two coordinated water molecules and two lattice water molecules in the asymmetric unit of compound **4**. The Co(II) atom is six-coordinated in a distorted octahedral coordination geometry, with the equatorial sites occupied by two oxygen atoms from two coordinated water molecules and two nitrogen atoms from two bpy ligands. The two axial sites are taken up by two oxygen atoms from two Hdpd⁻ ligands. The Co–O bond lengths are in the range of 2.104 to 2.113 Å, and the Co–N bond lengths are 2.139 and 2.153 Å. The Hdpd⁻ ligand in compound **5** is partially deprotonated, and adopts a unidentate coordination mode (Scheme 1d). Adjacent Co(II) atoms are connected by bpy ligands into an infinite 1D linear chain with a Co···Co distance of 11.356 Å (Fig. 4b). Since the Hdpd⁻ ligand is partially deprotonated and the terminal water molecules occupy two coordination nodes of the Co(II) atoms, these two factors together prevent the linkage between adjacent chains into higher dimensional structure. Adjacent 1D chains are held together through the hydrogen bonding interactions to form a 2D supramolecular layer (Fig. 4c).

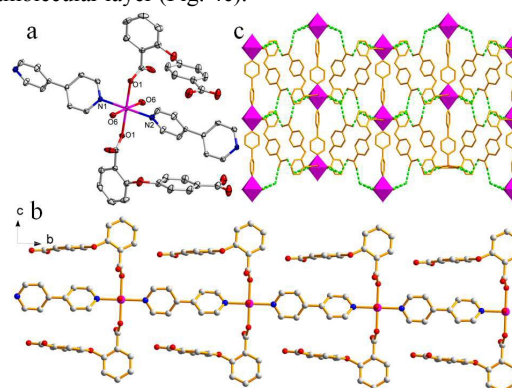


Fig. 4 (a) The coordination environment of Co(II) with the ellipsoids drawn at the 30% probability level. (b) 1D linear chain of **4**. (c) 2D supramolecular layer of **4** formed through hydrogen bonding.

The effects of coordination modes of H₂dpd ligand and reaction temperature on the final structures of compounds

Compared among the structures of compounds **1–5**, it is found that the reaction temperature and coordination modes of flexible H₂dpd ligand have important effects on the final structures of compounds **1–5**. For **1–5**, we selected different reaction temperatures (160 °C for **1**, **3** and 110 °C for **2**, **4** and **5**) while other reaction conditions are same. It is obvious that compounds **1** and **3** have higher dimensional structures than **2**, **4** and **5**. Since the flexible H₂dpd ligand was chosen as a main ligand in the formation of these compounds, it is very easy tune into different conformation modes in the self-assembly process of these compounds. Thus diverse dimensional structures can be obtained. Compound **1** shows 3D frameworks, while compound **3** is a 2D ladder layer. The coordination mode of the flexible H₂dpd ligand in compound **1** is chelating and bridging, which leads **1** to a 3D framework (Scheme 1a). In compound **3**, two independent Hdpd⁻ ligand and dpd²⁻ ligand show different coordination modes: one bridges two Co(II) atoms with chelating and monodentate modes (Scheme 1b), while the other one bridges one Co(II) atom with chelating modes (Scheme 1c) which prevents the linkage between the adjacent layers of **3** into high dimensional structure. Compound **2** shows a mononuclear structure, while the H₂dpd

ligand in **2** is partially deprotonated and one carboxyl group exhibits a chelating coordination mode (Scheme 1c). As for compounds **4** and **5**, they show an isostructural 1D linear chain structure, and the partially deprotonated ligand shows a monodentate coordination mode (Scheme 1d). Compared with compounds **4** and **5**, two coordination modes of Zn(II) atom in **2** are chelated by the Hdpd⁻ ligand, which prevent the mononuclear of **2** into a higher dimensional structure. In these manners, the coordination modes of the flexible ligand and reaction temperature impose a remarkable effect on the various dimensional structures of the compounds.

Thermogravimetric Analysis

To study the thermal stabilities of compounds **1** and **3–5**, TGA was performed in the temperature of 30–600 °C (see Fig. 5). Compound **1** remains stability up to 390 °C, and then it starts to decompose. The TGA curve of **3** shows a weight loss of 4.81% before 128 °C, corresponding to the removal of four water molecules (calculated: 4.13%). After the loss of all the free water molecules, the framework is stable up to 220 °C and begins to decompose upon further heating. For **4** and **5**, weight losses of 8.65% and 8.54% were observed in the temperature range of 30–120 °C and 30–126 °C, respectively, corresponding to the loss of two coordinated water molecules and two lattice water molecules (calculated: 8.99% and 8.99%, respectively). The residual compounds begin to decompose at 210 °C and 270 °C, respectively.

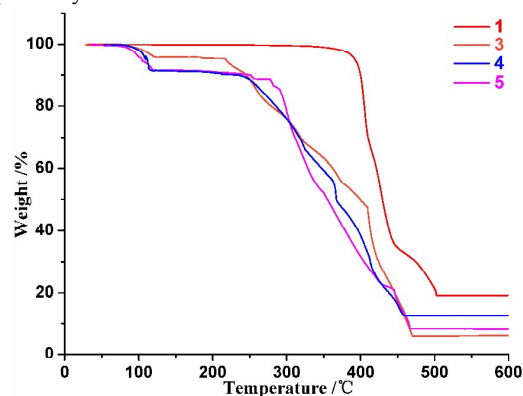


Fig. 5 TGA curves for compounds 1–5.

Fluorescence properties

The solid-state emission spectra of compounds **1** and **3–5** with H₂dpd and bpy ligands have been investigated at room temperature. As shown in Fig. 6, the main emission peaks of free H₂dpd, bpy ligands are at 361, 395 nm ($\lambda_{\text{ex}} = 250$ nm), respectively, which may be to the $\pi^*-\pi$ or π^*-n transitions of the intraligands.¹⁷ The emission peaks are at 381 nm in compound **1**, 392 nm in compound **3**, 395 nm in compound **4** and 412 nm in compound **5** upon excitation of solid samples at 270 nm. The emissions of these compounds may be assigned to the cooperative effects of intraligand transition and ligand-to-metal transfer.¹⁸ In comparison with the free ligands, the emission peaks in these compounds exhibit red shifts of different degree, which may be assigned to the differences of the coordination environment and the structures because the photoluminescence behavior is closely associated with the coordinated ligands and metal ions.¹⁹

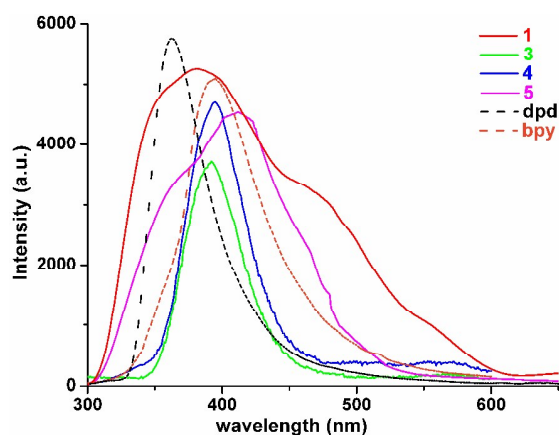


Fig. 6 Solid state emission spectra of compounds 1–5 at room temperature.

Water vapor sorption

Since there are many interstitial and coordinated water molecules in compounds **3–5**, we tried to study the sorption properties and reversibility of these compounds. From the TGA studies, the solvent molecules could be removed by heating the samples above 120 °C. Thus, we measured the water vapor sorption behaviour of **3–5**. Before the measurements, samples of these compounds were heated at 120 °C for 12 h under vacuum to remove the guest molecules trapped inside the pores. Water vapor sorption isotherms at 298 K are presented in Fig. 7. All these compounds exhibited gradual uptakes of water molecules and reached maximum values of 100.71 ml/g (**3**), 109.94 ml/g (**4**) and 108.96 ml/g (**5**) at $P/P_0 = 0.95$ (P_0 is the saturation pressure of H₂O at 298K), respectively, which are very high adsorption values. Due to the high polarity, water molecules can interact with the carboxyl groups from the dpd²⁻ ligand and nitrogen atoms from the bpy ligand in the structures via hydrogen bonding interactions.²¹ Thus, the obvious hysteresis for the desorption isotherms of **3–5** may suggest that the water molecules are strongly adsorbed in the pores of these compounds because of the hydrogen bonds. According to these compounds, the selection toward the carboxylate-based ligand has an important effect on desorption, which may expand the applicability for water sorption-based storage materials.

Magnetic property

The variable-temperature direct current (dc) magnetic susceptibility of compound **3** was measured under the 1000 Oe applied field in the temperature range of 2–300 K, which is shown as plots of $1/\chi_m$ versus T and $\chi_m T$ versus T in Fig. 8. The $\chi_m T$ value of **3** at 300 K of 8.249 cm³ mol⁻¹ K is larger than the expected of two spin only HS (High-spin) Cobalt(II) ($S = 3/2$) value of 3.75 cm³ K mol⁻¹ with $g = 2.0$, owing to the significant orbital contribution characteristics for the HS Co(II) ions.²⁰ The $\chi_m T$ value first smoothly decreases down to 120 K upon cooling, reaching a minimum value of 5.103 cm³ K mol⁻¹ at 2 K. This feature indicates antiferromagnetic couplings. In the range of 50 K to 300 K, the fitting $1/\chi_m$ data according to Curie-Weiss Law of $1/\chi_m = (T - \theta)/C$ gives Curie constant $C = 8.54$ cm³ K mol⁻¹ and Weiss constant $\theta = -7.01$ K, which indicates an antiferromagnetic interaction in compound **3**.

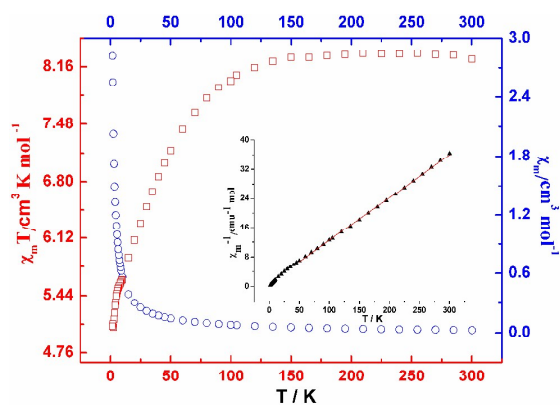


Fig. 8 Temperature dependence of magnetic susceptibilities in the form of the χ_m and $\chi_m T$ versus T for **3** at 1000 Oe. Inset: χ_m^{-1} versus T ; the solid line is fit to the experimental data.

For compound **4**, the $\chi_m T$ value at room temperature ($3.021 \text{ cm}^3 \text{ mol}^{-1} \text{ K}$ at 300 K) is higher than the expected spin-only value for one HS Co(II) ($S = 3/2$) ($1.875 \text{ cm}^3 \text{ mol}^{-1} \text{ K}$, $g = 2.0$), which is due to the orbital contribution of the HS Co(II) in the octahedral geometry (Fig. 9).²⁰ The value of $\chi_m T$ undergoes a steady decrease with decreasing temperature up to $1.669 \text{ cm}^3 \text{ mol}^{-1} \text{ K}$ at 2 K. The fitting $1/\chi_m$ data according to the Curie–Weiss Law gives Curie constant $C = 3.336 \text{ cm}^3 \text{ K mol}^{-1}$ and Weiss constant $\theta = -25.95 \text{ K}$. The negative Weiss constant suggests the existence of antiferromagnetic interaction in compound **4**.

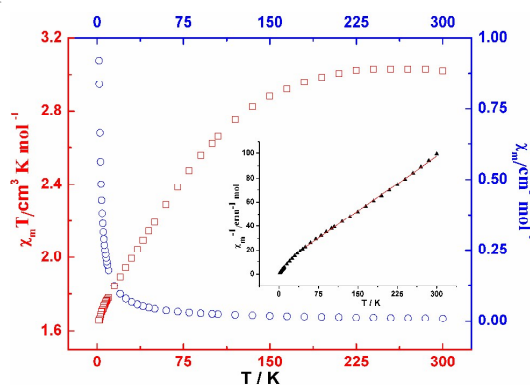


Fig. 9 Temperature dependence of magnetic susceptibilities in the form of the χ_m and $\chi_m T$ versus T for **4** at 1000 Oe. Inset: χ_m^{-1} versus T ; the solid line is fit to the experimental data.

For compound **5**, the $1/\chi_m$ versus T plot displays Curie–Weiss behavior from 300 to 50 K, the best linear fit of $\chi_m^{-1}(T)$ data above 50 K yields $C = 1.81 \text{ cm}^3 \text{ K mol}^{-1}$ and $\theta = 14.36 \text{ K}$ (Fig. 10). This positive Weiss constant indicates the presence of a ferromagnetic interaction between Ni(II) centers through the intermolecular interactions. The $\chi_m T$ value at 300 K is $1.85 \text{ cm}^3 \text{ K mol}^{-1}$, which is significantly larger than that expected for the contribution of one $S = 1$ Ni(II) center ($g = 2.2$). This was mainly attributed to the effects of spin–orbit coupling from the Ni(II) octahedral compound. Such a spin–orbit coupling also cause the g value to deviate the free ion value. Upon cooling the $\chi_m T$ value exhibits a rapid increase until 20 K; this may be indicative of the occurrence of ferromagnetic interactions between the Ni (II) centers of one–dimensional molecular chains. At low temperature starting from 20 K, the $\chi_m T$ value sharply decreases to a minimum value of $1.63 \text{ cm}^3 \text{ K mol}^{-1}$ at 2 K; this is attributed to a significant

zero–field splitting.

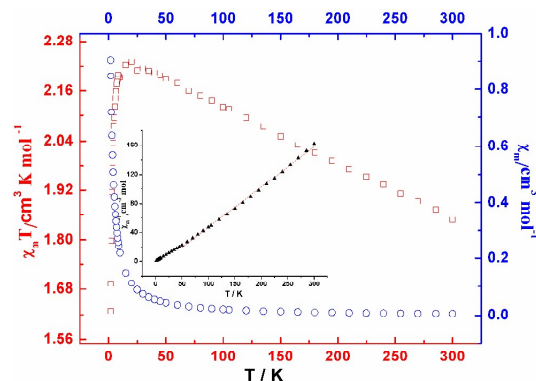


Fig. 10 Temperature dependence of magnetic susceptibilities in the form of the χ_m and $\chi_m T$ versus T for **5** at 1000 Oe. Inset: χ_m^{-1} versus T ; the solid line is fit to the experimental data.

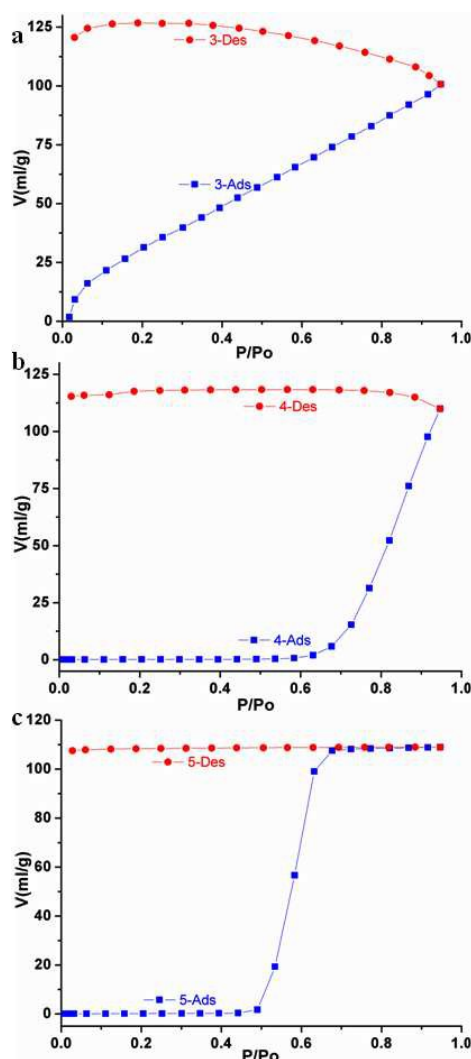


Fig. 7. Water adsorption-desorption isotherms for **3**, **4** and **5** at 298 K.

40 Conclusions

In summary, we have successfully synthesized and characterized five coordination polymers with zero-, one-, two- and

three-dimensional structures based on flexible H₂dpd ligand and different transition metal salts under similar hydrothermal conditions. According to the structures of these five compounds, we found that the final architectures can be influenced by different coordination modes of H₂dpd ligand and reaction temperatures. In addition, the thermal stabilities and fluorescence properties for compounds **1** and **3–5** have been investigated. The fluorescence behaviors indicate that red shifts of different degree may be assigned to the differences of the coordination environment and the structures which may indicate that these compounds can be good optical materials. Compounds **3–5** also show good water vapor uptakes, and the hysteresis of desorption isotherms of these compounds may suggest the applicability for water sorption-based storage materials. Moreover, magnetic studies reveal compound **3** and **4** show antiferromagnetic interaction, while compound **5** shows ferromagnetic behavior. This whole work evidently indicates that the effects of coordination modes of the flexible H₂dpd ligand and reaction temperatures are critical in construction of polymeric arrangement.

Acknowledgment

This work was financially supported by the National Nature Science Foundation of China (No. 21271024 and 20971014), supported by Beijing Natural Science (No 2112037), Foundation the 111 Project (B07012) in China, Foundation of the Open Project of Key Laboratory of Polyoxometalates Science of Ministry of Education of Northeast Normal University.

Notes and references

Key Laboratory of Cluster Science of Ministry of Education, School of Chemistry, Beijing Institute of Technology, Beijing 100081, PR China
E-mail: huangrudan1@bit.edu.cn

† Electronic Supplementary Information (ESI) available: X-ray crystallographic cif files, additional structural discription of compound **5**, selected bond lengths and angles and simulated and measured XRPD patterns, the studies of proton conductivity about compounds **3** and **3'**. Compounds **1–5** have been assigned the following numbers: CCDC 971571–971575, respectively.

- (a) C. Y. Lee, O. K. Farha, B. J. Hong, A. A. Sarjeant, S. T. Nguyen, J. T. Hupp, *J. Am. Chem. Soc.*, 2011, **133**, 15858; (b) Z. Y. Guo, H. Wu, G. Srinivas, Y. M. Zhou, S. C. Xiang, Z. X. Chen, Y. T. Yang, W. Zhou, M. O'Keefe, B. L. Chen, *Angew. Chem., Int. Ed.*, 2011, **50**, 3178; (c) J. R. Li, H. C. Zhou, *Nature*, 2010, **2**, 893; (d) Q. L. Zhu, W. Chu, R. D. Huang, L. J. Dong, X. Y. Cao, C. W. Hu, *Inorg. Chem. Commun.*, 2010, **13**, 1459; (e) N. Stock, S. Biswas, *Chem. Rev.*, 2012, **112**, 933; (f) R. B. Getman, Y. S. Bae, C. E. Wilmer, R. Q. Snurr, *Chem. Rev.*, 2012, **112**, 703; (g) M. P. Suh, H. J. Park, T. K. Prasad, D. W. Lim, *Chem. Rev.*, 2012, **112**, 782.
- (a) P. Lama, A. Aijaz, E. C. Sanudo, P. K. Bharadwaj, *Cryst. Growth Des.*, 2010, **10**, 283; (b) M. D. Allendorf, C. A. Bauer, R. K. Bhakta, R. J. T. Houk, *Chem. Soc. Rev.*, 2009, **38**, 1330; (d) L. J. Dong, W. Chu, Q. L. Zhu, R. D. Huang, *Cryst. Growth Des.*, 2011, **1**, 93; (d) Y. J. Cui, Y. F. Yue, G. D. Qian, B. Chen, *Chem. Rev.*, 2012, **112**, 1126; (e) C. A. Kent, D. Liu, T. J. Meyer, W. Lin, *J. Am. Chem. Soc.*, 2012, **134**, 3991.
- (a) L. Li, S. Wang, T. Chen, Z. Sun, J. Luo, M. Hong, *Cryst. Growth Des.*, 2012, **12**, 4109; (b) N. B. Shustova, B. D. McCarthy, M. Dinca, *J. Am. Chem. Soc.*, 2011, **133**, 20126; (c) J. Y. Lee, D. H. Olson, L. Pan, T. J. Emge, J. Li, *Adv. Funct. Mater.*, 2007, **17**, 1255; (d) D. Banerjee, S. J. Kim, W. Li, H. H. Wu, J. Li, L. A. Borkowski, B. L. Philips, J. B. Parise, *Cryst. Growth Des.*, 2010, **10**, 2801; (e) J. R. Li, J. Sculley, H. C. Zhou, *Chem. Rev.*, 2012, **112**, 869.
- (a) S. Su, Z. Guo, G. Li, R. Deng, S. Song, C. Qin, C. Pan, H. Guo, F. Cao, S. Wang, H. Zhang, *Dalton Trans.*, 2010, **39**, 9123; (b) M. Kurmoo, *Chem. Soc. Rev.*, 2009, **38**, 1353; (c) L. Zhang, G. C. Xu, H. B. Xu, T. Zhang, Z. M. Wang, M. Yuan, S. Gao, *Chem. Commun.*, 2010, **46**, 2554; (d) L. J. Dong, X. F. Li, J. Cao, W. Chu, R. D. Huang, *Dalton Trans.*, 2012, **42**, 1342.
- (a) R. Natarajan, G. Savitha, P. Dominiak, K. Wozniak, J. N. Moorthy, *Angew. Chem., Int. Ed.*, 2005, **44**, 2115; (b) J. J. Perry IV, J. A. M. J. P. Zaworotko, *Chem. Soc. Rev.*, 2009, **38**, 1400; (c) N. Stock, S. Biswas, *Chem. Rev.*, 2012, **112**, 933.
- (a) D. Wu, J. J. Gassensmith, D. Gouvêa, S. Ushakov, J. F. Stoddart, A. Navrotsky, *J. Am. Chem. Soc.*, 2013, **135**, 6790; (b) R. Heck, J. Bacsá, J. E. Warren, M. J. Rosseinsky, D. Bradshaw, *CrystEngComm*, 2008, **10**, 1687; (c) X. L. Wang, C. S. Qin, X. Wu, K. Z. Shao, Y. Q. Lan, S. Wang, D. X. Zhu, Z. M. Su, E. B. Wang, *Angew. Chem., Int. Ed.*, 2009, **48**, 5291; (d) F. Gross, E. Sherman, S. L. Mahoney, J. J. Vajo, *J. Phys. Chem. A*, 2013, **117**, 3771.
- (a) L. Ma, W. Lin, *J. Am. Chem. Soc.*, 2008, **130**, 13834; (b) X. Q. Lu, J. J. Jiang, C. L. Chen, B. S. Kang, C. Y. Su, *Inorg. Chem.*, 2005, **44**, 4515; (c) B. H. Zheng, J. Dong, Y. Li, S. Li, M. Scheer, *J. Am. Chem. Soc.*, 2008, **130**, 7778; (d) T. Ishiwata, Y. Furukawa, K. Sugikawa, K. Kokado, K. Sada, *J. Am. Chem. Soc.*, 2013, **135**, 5427.
- (a) B. Dey, S. R. Choudhury, P. A. Gamez, V. Vargiu, A. Robertazzi, C. Y. Chen, H. M. Lee, A. D. Jana, S. Mukhopadhyay, *J. Phys. Chem. A*, 2009, **113**, 8628; (b) A. Das, A. D. Jana, S. K. Seth, B. Dey, S. R. Choudhury, T. Kar, S. Mukhopadhyay, N. J. Singh, I. C. Hwang, K. S. Kim, *J. Phys. Chem., B*, 2010, **114**, 4166; (c) J. Canivet, S. Aguado, Y. Schuurman, D. Farrusseng, *J. Am. Chem. Soc.*, 2013, **135**, 4195.
- (a) X. Zhou, P. Liu, W. H. Huang, Y. Y. Wang, Q. Z. Shi, *CrystEngComm*, 2013, **15**, 8125; (b) Z. W. Wang, C. C. Ji, J. Li, Z. J. Guo, Y. Z. Li, H. G. Zheng, *Cryst. Growth Des.*, 2009, **9**, 475; (c) Y. Q. Lan, H. L. Jiang, S. L. Li, Q. Xu, *Inorg. Chem.*, 2012, **51**, 7484.
- (a) W. Zhao, J. Han, G. Tian, X. L. Zhao, *CrystEngComm*, 2013, **15**, 7522; (b) P. Kanoo, K. L. Gurunatha, T. K. Maji, *Cryst. Growth Des.*, 2009, **9**, 4147; (c) H. J. Li, B. Zhao, R. Ding, Y. Y. Jia, H. W. Hou, Y. T. Fan, *Cryst. Growth Des.*, 2012, **12**, 4170.
- (a) S. Kitagawa, R. Kitaura, S. Noro, *Angew. Chem., Int. Ed.*, 2004, **43**, 2334; (b) J. L. C. Rowsell, O. M. Yaghi, *Microporous Mesoporous Mater.*, 2004, **73**, 3.
- (a) L. L. Zhang, F. L. Liu, Y. Guo, X. P. Wang, Y. H. Wei, Z. Chen, D. F. Sun, *Cryst. Growth Des.*, 2012, **12**, 6215; (b) A. M. Fonseca, M. M. M. Raposo, A. M. R. C. Sousa, G. Kirsch, M. Beley, *Eur. J. Inorg. Chem.*, 2005, **21**, 4361; (c) C. Pettinari, N. Masciocchi, L. Pandolfo, D. Pucci, *Chem. Eur. J.*, 2010, **16**, 1106; (d) H. Y. Zang, Y. Q. Lan, G. S. Yang, X. L. Wang, K. Z. Shao, G. J. Xu, Z. M. Su, *CrystEngComm*, 2010, **12**, 434; (e) S. Verma, A. K. Mishra, J. Kumar, *Acc. Chem. Res.*, 2010, **43**, 79.
- X. Y. Cao, B. Mu, R. D. Huang, *CrystEngComm*, 2014, **16**, 5093.
- G. M. Sheldrick, SADABS: Empirical Absorption Correction Program, University of Göttingen: Göttingen, Germany, 1997.
- XPREP, version 5.1. Siemens Industrial Automation Inc.: Madison, WI, 1995.
- G. M. Sheldrick, SHELXS-97, Program for Crystal Structure Solution; Gottingen University: Germany, 1997.
- (a) J. Yang, Q. Yue, G. D. Li, J. J. Cao, H. G. Li, J. S. Chen, *Inorg. Chem.*, 2006, **45**, 2857; (b) X. J. Zhang, L. P. Jin, S. Gao, *Inorg. Chem.*, 2004, **43**, 1600.
- (a) X. Ting, *J. Inorg. Organomet Polym.*, 2012, **22**, 386; (b) J. Tao, M. L. Tong, J. X. Shi, X. M. Chen, S. W. Ng, *Chem. Commun.*, 2000, 2043; (c) Z. Su, J. Xu, J. Fan, D. J. Liu, Q. Chu, M. S. Chen, S. S. Chen, G. X. Liu, X. F. Wang, W. Y. Sun, *Cryst. Growth Des.*, 2009, **9**, 2801.
- (a) J. C. Dai, X. T. Wu, Z. Y. Fu, C. P. Cui, S. M. Hu, W. X. Du, L. M. Wu, H. H. Zhang, R. Q. Sun, *Inorg. Chem.*, 2002, **41**, 1391; (b) D. S. Raja, J. H. Luo, C. Y. Wu, Y. J. Cheng, C. T. Yeh, Y. T. Chen, S. H. Lo, Y. L. Lai, C. H. Lin, *Cryst. Growth Des.*, 2013, **13**, 3785.

-
- 20 (a) Y. F. Bi, X. T. Wang, W. P. Liao, X. F. Wang, X. W. Wang, H. J. Zhang, S. Gao, *J. Am. Chem. Soc.*, 2009, **131**, 11650.